Chinese Chemical Letters 36 (2025) 110289

Contents lists available at ScienceDirect

Chinese Chemical Letters

journal homepage: www.elsevier.com/locate/cclet

Tumor acidic microenvironment activatable DNA nanostructure for precise cancer cell targeting and inhibition

Yanfei Liu[b,1], Yaqin Hu[b,1], Yifu Tan[a], Qiwen Chen[b], Zhenbao Liu[a,c,*]

[a] Xiangya School of Pharmaceutical Sciences, Central South University, Changsha 410013, China
[b] Department of Pharmaceutical Engineering, College of Chemistry and Chemical Engineering, Central South University, Changsha 410083, China
[c] Molecular Imaging Research Center of Central South University, Changsha 410008, China

ARTICLE INFO

Article history:
Received 13 June 2024
Revised 18 July 2024
Accepted 22 July 2024
Available online 23 July 2024

Keywords:
Aptamer
i-motif
DNA nanostructure
Logic gate
Drug delivery system

ABSTRACT

Precise tumor targeting and therapy is a major trend in cancer treatment. Herein, we designed a tumor acidic microenvironment activatable drug loaded DNA nanostructure, in which, we made a clever use of the sequences of AS1411 and i-motif, which can partially hybridize, and designed a simple while robust DNA D-strand nanostructure, in which, i-motif sequence was designed to regulate the binding ability of the AS1411 aptamer to target tumor. In the normal physiological environment, i-motif inhibits the targeting ability of AS1411. In the acidic tumor microenvironment, i-motif forms a quadruplex conformation and dissociates from AS1411, restoring the targeting ability of AS1411. Only when acidic condition and tumor cell receptor are present, this nanostructure can be internalized by the tumor cells. Moreover, the structure change of this nanostructure can realize the release of loaded drug. This drug loaded A-I-Duplex DNA structure showed cancer cell and spheroid targeting and inhibition ability, which is promising in the clinical cancer therapy.

In cancer targeted therapy, it is essential to reduce the side effects of drug on normal cells. Precise tumor targeting and therapy is a major trend. Molecules that can smartly recognize tumor are usually employed. Constructing tumor environment activatable drug delivery systems is a new research direction. The nucleic acid aptamer is an oligonucleotide sequence screened by systematic evolution of ligands by exponential enrichment (SELEX) technique. Aptamer can bind to specific targets with high affinity and specificity [1]. Due to good biocompatibility and easy modifiability, aptamers are widely applied as targeting molecules in various drug delivery systems, such as drug molecules [2,3], nanoparticles [4], liposomes [5], inorganic materials [6-8], exosomes [9], nucleic acid nanostructures [10], and in diagnostics [11-14]. Aptamers reduce the side effects through binding with the biomarkers overexpressed on the surface of tumor cells. However, tumor biomarkers are also expressed at low level on the surface of normal cells, resulting in toxicity to normal cells during cancer therapy. Therefore, developing new intelligent aptamers to enhance targeting precision and reduce side effects is currently a key issue that needs to be addressed. Here, we proposed the concept of inhibiting the targeting ability of aptamers under normal physiological conditions, while restoring the targeting ability of aptamers in the tumor microenvironment, thereby improving the tumor targeting accuracy.

The microenvironment is an important characteristic of tumor. Due to the hypoxic state of the tumor microenvironment and the fast metabolism of cancer, the significant accumulation of hydrogen ion makes the tumor microenvironment acidic [15]. Utilizing the pH difference between the tumor microenvironment and the normal physiological environment, here, we designed a DNA strand containing pH-responsive i-motif to regulate the targeting ability of aptamer. The i-motif structure forms in cytosine-rich (C-rich) DNA sequences under slightly acidic conditions (pH 5.5–7.0), where cytosines protonate and pair to create a four-stranded helix [16]. In contrast, G-quadruplex structures form in guanine-rich sequences stabilized by Hoogsteen hydrogen bonding and cation coordination, typically under low pH and specific ion concentrations [17]. Considering the special C-rich sequence of i-motif, guanine-rich (G-rich) AS1411 was chosen as the targeting ligand. AS1411 is a 26-base G-rich oligonucleotide that can form G-quadruplex conformation, whose primary molecular target is nucleolin [18]. Nucleolin is one of the most abundant nucleolar proteins in the nucleus of normal cells and is overexpressed in the cytoplasm of metastatic and rapidly dividing cells, and on the cancer cell membrane [19]. It has been reported that AS1411 can bind to the nucleolin and

* Corresponding author.
E-mail address: zhenbaoliu@csu.edu.cn (Z. Liu).
[1] These authors contributed equally to this work.

https://doi.org/10.1016/j.cclet.2024.110289
1001-8417/

inhibit the cancer cells [20]. Here, we designed a functional strand S-I possessing potential i-motif structure, and 9-nt sequence of S-I is complementary to a part of AS1411 aptamer, and their combination was called A-I involving an "AND" gate. In normal physiological environment, the targeted ability of AS1411 is inhibited by S-I. In acid tumor microenvironment, i-motif structure thus separates from AS1411 and the targeting ability of AS1411 can be restored. Only when both H^+ and nucleolin are present, the AS1411 binds with the receptor and the S-I completely separates from AS1411.

Furthermore, we attached A-I to a DNA duplex to form A-I-Duplex for achieving targeted drug delivery (Fig. 1). The anticancer drug doxorubicin (Dox) was inserted in DNA duplex forming A-I-Duplex@Dox. The sequences are listed in Table S1 (Supporting information). Different from general drug delivery systems, the therapeutic target of A-I-Duplex@Dox is the tumor acidic microenvironment and tumor cell receptor. When A-I-Duplex@Dox reaches acidic tumor microenvironment, the formation of quadruplex of i-motif and the binding of aptamer with nucleolin lead to the dissociation of S-I and AS1411, thereby releasing part of the drugs and being taken up by tumor cells. The remaining drug was delivered into tumor cells along with A-I-Duplex, thus improving the treatment efficiency.

Preparation of A-I: Due to hypoxia and acidic intracellular organelles in the tumor, lactic acid is produced significantly, thus lowering the pH value of the tumor microenvironment compared to the normal physiological environment [21]. The normal physiological pH is around 7.4, while the pH value of tumor microenvironment is 6.5–7.2 [22]. Considering pH range surrounding tumor tissues, we chose the i-motif strand with responsive pH range between 6.4 and 7.0 and midpoint pH of 6.71 [23]. To improve the binding rate of S-I and AS1411 (S-A), a 9-base sequence that is complementary to AS1411 was added based on the i-motif sequence. The hybridization rate of S-I and S-A evaluated by NUPACK was up to 99% [24].

The assembly of A-I was verified by 20% native polyacrylamide gel electrophoresis (PAGE). The clear line 3 indicated high yield of A-I (Fig. S1A in Supporting information). The line 4 presents Ctrl-A-I (without pH responsiveness), assembled by S-A and complementary strand Ctrl-S-I, set as control group. To test the stability of A-I in acidic environment without nucleolin, we labeled 5′s end of S-A and 3′s end of S-I with Cy5 and BHQ2, respectively. Fluorescence quenching occurs when S-I and S-A are combined. When H^+ and nucleolin are present, the dissociation of the two strands leads to Cy5 fluorescence recovery. Fluorescently labeled A-I was equilibrated in phosphate buffered solution (PBS) at pH 7.4 or 6.5 for different times (Fig. S1B in Supporting information). Obvious fluorescence quenching indicated the successful hybridization of S-A and S-I. After equilibrium in buffer at pH 6.5 for 24 h, the fluorescence intensity of Cy5 of A-I in PBS at pH 6.5 remained consistent with A-I in PBS (pH 7.4), which indicated that A-I is stable in acidic environment.

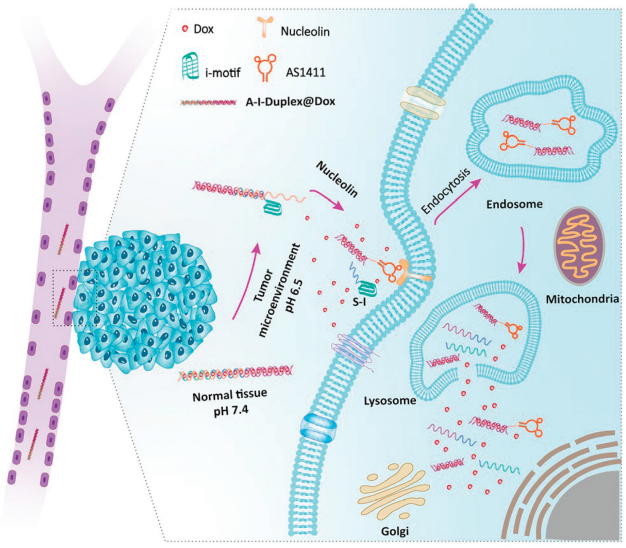

Fig. 1. Schematic diagram of cellular internalization and intracellular anti-cancer drug release of A-I-Duplex@Dox.

It was reported that the i-motif is able to perform proton response when it is partly paired forming duplex [25,26]. To further verify the proton response ability of i-motif in the acidic environment after the formation of the duplex, circular dichroism (CD) spectroscopy was used to identify the structural changes of A-I at different pH values. As shown in Fig. S1C (Supporting information), in pH 7.4 PBS, the A-I showed positive and negative peaks at 265 and 238 nm, which were similar to the characteristic CD spectra of B-DNA duplex, while spectra of A-I at pH 6.5 showed positive and negative peaks at 280 and 238 nm, which means that the conformational change of A-I was happened when pH changed, suggesting the i-motif in A-I duplex was still able to perform proton response [27]. In control group, the characteristic peaks of Ctrl-A-I in CD spectrum at different pH environments did not change (Fig. S1D in Supporting information).

Verification of the logic gate of A-I: To test the pH actuation and nucleolin actuation of A-I, we labeled S-A and S-I with Cy5 and BHQ2, respectively, for monitoring the cellular uptake of A-I. The Ctrl-A-I was set as control to eliminate the non-specific adsorption factors of cells to the sample, and the targeting ability of S-A is completely inhibited in Ctrl-A-I. Samples were incubated with nucleolin-positive A549 and nucleolin-negative L02 cells for 15 min. The amount of delivered sample was estimated by the fluorescence intensity of the Cy5. As shown in Fig. 2A, in control groups, both A549 and L02 cells exhibited no obvious uptake of Ctrl-A-I, suggesting that the targeting function of AS1411 was severely inhibited in Ctrl-A-I. In experimental groups, the A549 cells in acidic media exhibited significantly higher fluorescence than the cells in neutral media, which verified the i-motif separated from AS1411 to form quadruplex in acidic environment, and the targeted ability of AS1411 was restored. In addition, the fluorescence intensities of L02 cells in acidic and neutral media were much lower, and showed no significant difference, which further indicated that A-I had good stability under acidic conditions, and most A-I retained double-stranded configuration in the absence of nucleolin.

In order to eliminate the factor of uptake difference in uptake between different cells, and to more intuitively and quantitatively reflect the uptake of samples by cells, flow cytometry experiment was conducted to detect the fluorescence intensity of each cell under different conditions (Fig. 2B). According to the experimental results, the fluorescence intensity of A549 cells treated by A-I at pH 6.5 was significantly stronger than that at pH 7.4, indicating that the targeting ability of AS1411 in A-I in acidic environment was much stronger than that in neutral environment. Furthermore, pH-dependent uptake was observed in L02 cells. Both A549 and L02 cells showed low uptake of Ctrl-A-I, and there was negligible change of intracellular fluorescence between pH 7.4 and pH 6.5. The flow cytometry result was basically consistent with the result of the cell uptake experiment. In addition, to further verify the regulatory effect of i-motif on the targeting ability of AS1411, we also verified the pH actuation of A-I on nucleolin-positive HeLa cells. The results of cellular uptake and flow cytometry experiments on HeLa cells showed pH-dependent phenomenon (Fig. S2 in Supporting information). Therefore, the above experiments verified the

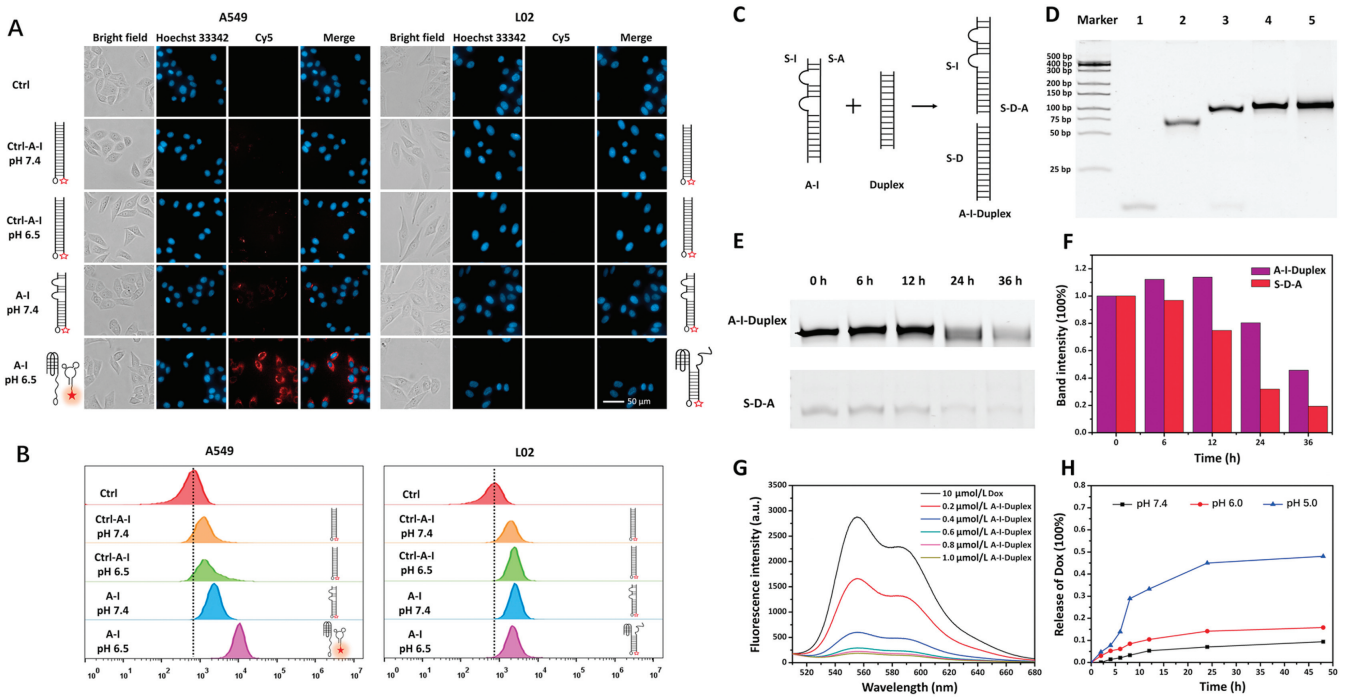

Fig. 2. Verification of the "AND" gate of A-I. (A) High content images of A549 cells and L02 cells incubated with different samples (500 nmol/L) for 15 min. The small pictures on both sides represent the different states of the samples under different conditions. The black ellipse and the red star represent BHQ2 and Cy5, respectively. (B) Flow cytometry of Ctrl-A-I and A-I (500 nmol/L) were incubated with A549 and L02 cells, respectively, for 15 min. (C) Schematic diagram of A-I-Duplex. (D) The PAGE image of A-I-Duplex analysis the stability of A-I-Duplex in media containing 10% FBS. Lanes 1–5: S-D, S-D-A, S-D + S-D-A, A-I-Duplex, Ctrl-A-I-Duplex, respectively. (E) PAGE analysis of A-I-Duplex and S-D-A in 10% FBS DMEM for different time. (F) Band intensity of the gel electrophoresis images in (E). (G) The drug loading profiles of A-I-Duplex. (H) The release profiles of A-I-Duplex@Dox in PBS at different pH values. Scale bar: 50 μm.

feasibility of the "AND" gate of A-I. To some extent, the i-motif can regulate the targeting function of aptamer AS1411.

Preparation and stability of A-I-Duplex: In drug delivery field, DNA structure is an excellent tool for drug delivery due to good biocompatibility [28]. We decided to apply A-I into DNA duplex forming A-I-Duplex for targeted drug delivery. As shown in Fig. 2C, A-I-Duplex was assembled by three strands: S-I, S-D-A containing S-A, and S-D. The gel electrophoresis analysis exhibited one obvious band for each intermediate in the assembly of A-I-Duplex (Fig. 2D), suggesting successful construction of the functional nanostructure.

Aptamer has relatively poor biostability due to nuclease hydrolysis *in vivo*. Chemical modification is a common strategy to improve the biostability of aptamer, such as terminal modification to block the exonuclease attack [29], modification on the nucleic acid backbone of aptamer [30,31], conjugation of aptamer to nanoparticles [32]. The aptamer is easily compatible with the nucleic acid structure, utilizing nucleic acid structure to protect aptamer is also a common method. Previous studies have proven that dsDNA is more stable than ssDNA in biological media. Therefore, to test the stability of A-I-Duplex *in vivo*, we incubated S-D-A and A-I-Duplex with the same concentration in DMEM media containing 10% fetal bovine serum (FBS) for different times, respectively. Then, structural integrity of them was characterized *via* 20% native PAGE (Fig. 2E). The result showed that the majority of A-I-Duplex remained stable after 12 h incubation, while S-D-A started to degrade. After 24 h incubation, the remaining amount of A-I-Duplex was basically twice that of S-D-A (Fig. 2F). From the results above, A-I-Duplex was more stable than S-D-A, and the duplex structure of A-I-Duplex showed protection effect to aptamer in biological media.

Drug loading and *in vitro* drug release: Theoretically, Dox is mainly embedded in the G–C sequences of the DNA backbone [33,34]. The fluorescence quenching occurs when Dox is inserted into the DNA duplex. When the ratio of A-I-Duplex to Dox was 1:12.5 and 1:10, the fluorescence curves were substantially coincident and fluorescence of Dox was nearly quenched, which meant that the drug loading has reached saturation (Fig. 2G). Thus, the ratio of A-I-Duplex to Dox was 1:12.5. The A-I and Ctrl-A-I-D to Dox ratio were 1:5 and 1:12.5, respectively, which means that the drug in A-I-Duplex@Dox released outside tumor cells was approximately 40% (Fig. S3 in Supporting information). Additionally, we evaluated the release of Dox from A-I-Duplex in PBS at different pH (pH 7.4, 6.0 and 5.0). As shown in Fig. 2H, the release of drug reached equilibrium at 24 h. For 48 h, less than 10% of Dox was released from A-I-Duplex at pH 7.4 (physiological environment) and the release rate of Dox at pH 6.0 was less than 20%. At pH 5.0, close to the pH of lysosomes in tumor cells, the drug release efficiency reached about 48% after 48 h, which suggested that the release of drug gradually increased with the internalization of tumor cells in lysosomes.

In vitro cellular uptake of A-I-Duplex@Dox: To test whether the logic gate will be affected after the linkage of A-I and duplex, the cellular uptake of A-I-Duplex@Dox was studied. The drug release of A-I-Duplex@Dox includes extracellular and intracellular drug release. When A-I-Duplex@Dox arrived at acidic tumor microenvironment, S-I dissociated from AS1411 because of proton response and the combination of aptamer and nucleolin, resulting in the release of a small amount of Dox outside cells. And then, A-I-Duplex@Dox was internalized by cells *via* nucleolin-mediated pathway to bring the remaining drugs into the tumor cells. As shown in Fig. 3A, compared to A549 cells treated with A-I-Duplex@Dox at pH 7.4, the fluorescence intensity of A549 cells treated by A-I-Duplex@Dox at pH 6.5 was obviously stronger, and the cellular uptake of A-I-Duplex@Dox by L02 cells at pH 7.4 and 6.5 was lit-

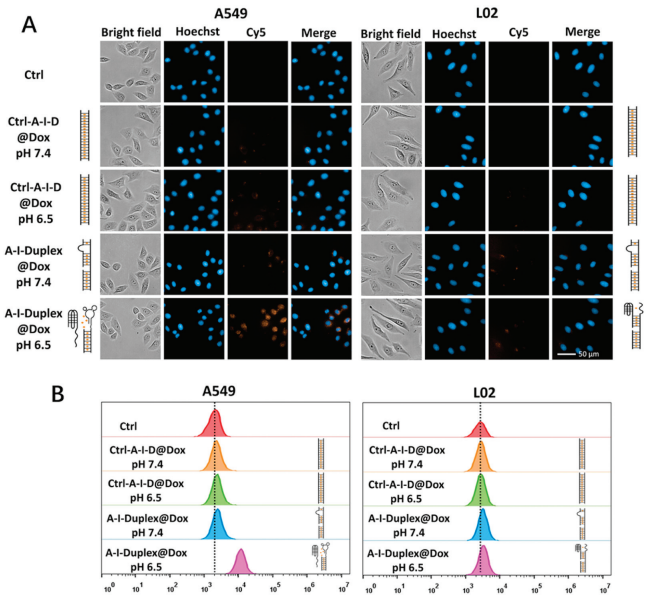

Fig. 3. (A) Fluorescent images of cells incubated by different samples at pH 7.4 or 6.5. (B) Flow cytometry of A549 and L02 cells after incubation with different samples for 30 min. Scale bar: 50 μm.

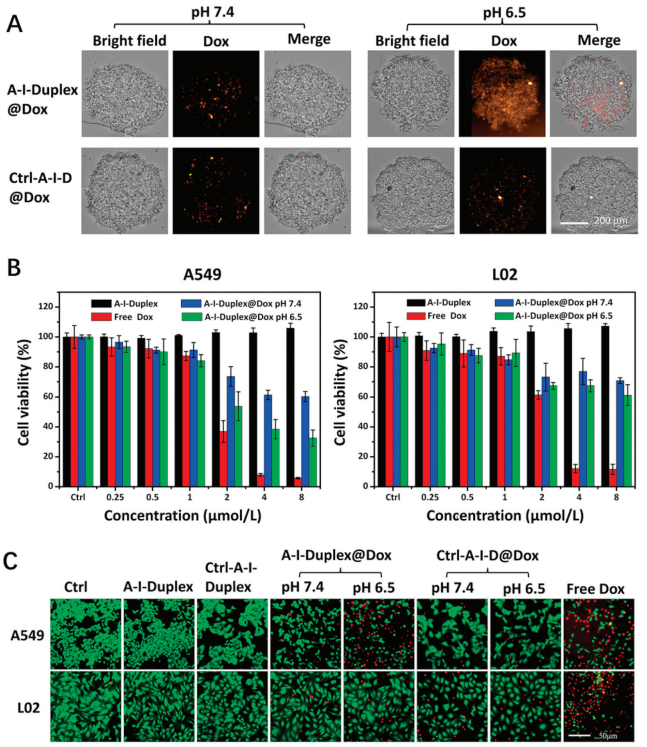

Fig. 4. (A) Tumor spheroids incubated with 4 μmol/L samples (A-I-Duplex@Dox pH 7.4, A-I-Duplex@Dox pH 6.5, Ctrl-A-I-D@Dox pH 7.4, Ctrl-A-I-D@Dox pH 6.5) for 1 h, respectively. Scale bar: 200 μm. (B) Cytotoxicity of free Dox, A-I-Duplex, A-I-Duplex@Dox pH 7.4 and A-I-Duplex@Dox pH 6.5 to A549 and L02 cells. (C) Calcein-AM/PI double staining assays on A549 cells and L02 cells treated by different samples after 24 h. Scale bar: 50 μm. Data are presented as mean ± standard deviation (SD) ($n = 5$).

tle. Furthermore, the accumulations of Dox in A549 and L02 cells treated with Ctrl-A-I-D@Dox were low.

In flow cytometry analysis, A549 cells treated by the experimental samples (A-I-Duplex@Dox pH 7.4, A-I-Duplex@Dox pH 6.5) exhibited pH-dependent uptake, while that feature did not exhibit in L02 cells (Fig. 3B). The A549 and L02 showed no obvious difference in the uptake of Ctrl-A-I-D and A-I-Duplex at pH 7.4. Comparing the results of the two flow cytometry analyses (Figs. 2B and 3B), we can find that the cells showed a certain uptake to Ctrl-A-I, but almost no uptake of Ctrl-A-I-D@Dox, which may be due to the fact that the Ctrl-A-I-D is more negative charged than that of Ctrl-A-I, making Ctrl-A-I-D@Dox more difficult to enter into cancer cells. From the above results. A-I-Duplex showed pH-dependent behavior and specificity to tumor cells. Moreover, the logic gate of A-I-Duplex still works.

Uptake and therapeutic effect on multicellular tumor spheroids: Two-dimensional cell culture cannot provide a true and complex microenvironment for cells. In order to restore the true situation of tumors in the body as much as possible, we constructed a multi-cell tumor spheroids model to simulate the real situation of tumor tissues in the body. The penetration ability of drugs into tumor spheroids is the key for therapeutic effect. Large particle will lead to difficulty in penetration and low uptake of tumor cells, resulting in poor therapeutic effect. The size of A-I-Duplex is less than 10 nm, theoretically, the penetration ability is relatively strong. Here, we mainly studied different uptake of A-I-Duplex@Dox at different pH by tumor spheroids. As shown in the Fig. 4A, in the experimental groups treated with A-I-Duplex@Dox, the fluorescence of the tumor spheroid in pH 6.5 was significantly stronger than that in pH 7.4, indicating that the accumulation of Dox in the tumor spheroid in the acidic environment was higher. Because the targeting ability of aptamer was inhibited in the neutral environment, but restored in acidic environment, enhancing the uptake of A-I-Duplex@Dox by cancer cells. In addition, the tumor spheroids treated by Ctrl-A-I-D@Dox pH 7.4 and Ctrl-A-I-D@Dox pH 6.5 showed weak fluorescence, which demonstrated that the targeting ability of AS1411 was severely inhibited when AS1411 was fully hybridized.

Antitumor efficacy of A-I-Duplex@Dox *in vitro*: The difference of cytotoxicity of A-I-Duplex@Dox in pH 7.4 and 6.5 environment was evaluated by cell-counting kit (CCK-8). From the cell viability assay, >95% cells incubated with A-I-Duplex were living, suggesting that the cytotoxicity of A-I-Duplex was negligible (Fig. 4B). In a Dox concentration range of 0.25–1 μmol/L, the three groups (free Dox, A-I-Duplex@Dox pH 7.4, A-I-Duplex@Dox pH 6.5) induced apoptosis with no significant difference. When the concentration goes beyond 1 μmol/L, the viability of A549 cells treated by A-I-Duplex@Dox pH 6.5 was obviously lower than that of cells treated by A-I-Duplex@Dox pH 7.4, which meant the A-I-Duplex did realize high precise drug delivery. By contrast, for L02 cells, with the increase of concentrations, the cytotoxicity of A-I-Duplex@Dox was basically independent of pH value. By calculation, the IC_{50} value of A-I-Duplex@Dox at pH 6.5 for A549 cells is about 4.6 μmol/L, which is lower than that of Dox for A549 cells (2.1 μmol/L). There may be two reasons: (1) the dissociation rate of S-I and AS1411 does not reach 100% at pH 6.5, which results in a part of the targeting ability of AS1411 being inhibited; (2) the surface of nucleic acid is negatively charged, which makes A-I-Duplex@Dox have a lower uptake than free Dox. As for control group, Ctrl-A-I-D@Dox had no significant difference in cytotoxicity at different pH, and exhibited no pH-dependent and nucleolin-dependent behaviors (Fig. S4 in Supporting information). The above results indicate that the targeting ability of AS1411 in Ctrl-A-I-D is greatly inhibited. Thus, the cytotoxicity assay further verified that the i-motif did can regulate the targeting ability of AS1411, and A-I-Duplex@Dox achieved targeted drug delivery with high precision.

To visualize cytotoxicity efficiency, cells treated by different samples were stained by calcein-AM/propidium iodide (PI) reagent, in which calcein-AM was used for fluorescently labeling living cells

(green) and PI for staining dead cells (red). Based on cytotoxicity experiment results, the cytotoxicity of A-I-Duplex@Dox was not much different at 4 and 8 μmol/L. Therefore, the concentration of samples in double staining experiment was determined as 4 μmol/L. As shown in Fig. 4C, in A549 cells group, from the ratio of red to green, the dead cells in cell group treated by A-I-Duplex@Dox at pH 6.5 was more than group treated by A-I-Duplex@Dox at pH 7.4. The number of dead cells in L02 cell groups incubated by A-I-Duplex@Dox did not differ much. The toxicity of Ctrl-A-I-D@Dox to the two kinds of cells did not show any difference in pH. Therefore, the results of the double staining experiment are basically consistent with the results of the cytotoxicity experiment.

In summary, taking advantage of the characteristics of the acidic tumor microenvironment, we designed a functional strand S-I to regulate the targeting ability of AS1411. The targeting ability of AS1411 was inhibited in normal physiological environment, but restored in acidic tumor microenvironment. Dual targets of tumor microenvironment and tumor cells have improved the accuracy of targeting. Moreover, drug delivery system showed high precise tumor cell targeting ability, achieving dual targeted drug delivery of tumor cells and tumor microenvironment, providing a new idea for realizing high-precision and high-efficiency tumor treatment. We utilized the C-rich functional nucleic acid i-motif to complement the G-rich AS1411 to regulate the targeting function of the AS1411, that idea can be extended to other aptamers, for i-motifs with appropriate sequences or other functional molecules to regulate the targeting function of the aptamers. Future work should explore extending this strategy to diverse aptamers and nucleic acids, and *in vivo* experiments will contribute to advancing this strategy towards clinical applications.

Declaration of competing interest

The authors declare that they have no known competing financial interests or personal relationships that could have appeared to influence the work reported in this paper.

CRediT authorship contribution statement

Yanfei Liu: Writing – original draft, Methodology, Investigation, Conceptualization. **Yaqin Hu:** Writing – original draft, Investigation, Funding acquisition, Conceptualization. **Yifu Tan:** Methodology, Investigation. **Qiwen Chen:** Methodology, Investigation. **Zhenbao Liu:** Writing – review & editing, Supervision, Methodology, Investigation, Funding acquisition, Formal analysis, Conceptualization.

Acknowledgments

This research was funded by the National Natural Science Foundation of China (No. 32271464), the Hunan Provincial Natural Science Foundation for Distinguished Young Scholars (No. 2022JJ10086), the Innovation-Driven Project of Central South University (No. 2020CX048), HunanProvincial High-Level Health Talents (No. 20240304088). The Joint Fund of the Hunan Provincial Natural Science Foundation and the Hunan Medical Products Administration (No. 2023JJ60501).

Supplementary materials

Supplementary material associated with this article can be found, in the online version, at doi:10.1016/j.cclet.2024.110289.

References

[1] C. Tuerk, L. Gold, Science 249 (1990) 505–510.
[2] A. Pusuluri, V. Krishnan, V. Lensch, et al., Angew. Chem. Int. Ed. 58 (2019) 1437–1441.
[3] H. Xiong, J. Yan, S. Cai, et al., Mol. Pharm. 17 (2020) 2882–2890.
[4] X. Sun, B. Liu, X. Chen, et al., J. Mater. Sci. Mater. Med. 30 (2019) 76.
[5] Q. Ma, W. Qian, W. Tao, Y. Zhou, B. Xue, Drug Des. Devel. Ther. 13 (2019) 4021–4033.
[6] W.H. Chen, O. Karmi, B. Willner, R. Nechushtai, I. Willner, Sensors 19 (2019) 5260.
[7] S. Cai, J. Yan, H. Xiong, et al., Int. J. Pharm. 590 (2020) 119948.
[8] N. Zhao, J. Coyne, L. Abune, et al., ACS Appl. Mater. Interfaces 12 (2020) 24599–24610.
[9] J. Zou, M. Shi, X. Liu, et al., Anal. Chem. 91 (2019) 2425–2430.
[10] Y. Zhan, W. Ma, Y. Zhang, et al., ACS Appl. Mater. Interfaces 11 (2019) 15354–15369.
[11] L. Li, J. Wang, H. Jiang, et al., Chin. Chem. Lett. 34 (2023) 107506.
[12] Y. Zhang, Y. Liu, Y. Yang, et al., Chin. Chem. Lett. 34 (2023) 108102.
[13] L. Zhao, F. Ahmed, H. Xiong, Chin. Chem. Lett. 33 (2022) 4243–4247.
[14] J. Jouha, F. Li, H. Xiong, Spectrochim. Acta A: Mol. Biomol. Spectrosc. 295 (2023) 122615.
[15] A. Hulikova, P. Swietach, FASEB J. 28 (2014) 2762–2774.
[16] D. Hanahan, R.A. Weinberg, Cell 144 (2011) 646–674.
[17] D. Sen, W. Gilbert, Nature 334 (1988) 364–366.
[18] P.J. Bates, D.A. Laber, D.M. Miller, S.D. Thomas, J.O. Trent, Exp. Mol. Pathol. 86 (2009) 151–164.
[19] X. Chen, D.M. Kube, M.J. Cooper, P.B. Davis, Mol. Ther. 16 (2008) 333–342.
[20] S. Soundararajan, W. Chen, E.K. Spicer, N. Courtenay-Luck, D.J. Fernandes, Cancer Res. 68 (2008) 2358–2365.
[21] I. Mellman, R. Fuchs, A. Helenius, Annu. Rev. Biochem. 55 (1986) 663–700.
[22] C. Nilsson, K. Kagedal, U. Johansson, K. Ollinger, Methods Cell Sci. 25 (2003) 185–194.
[23] I.V. Nesterova, E.E. Nesterov, J. Am. Chem. Soc. 136 (2014) 8843–8846.
[24] J.N. Zadeh, C.D. Steenberg, J.S. Bois, et al., J. Comput. Chem. 32 (2011) 170–173.
[25] J. Kim, C. Jo, W.G. Lim, et al., Adv. Mater. 30 (2018) 1707557.
[26] S.H. Kim, K.R. Kim, D.R. Ahn, et al., ACS Nano 11 (2017) 9352–9359.
[27] K. Leung, K. Chakraborty, A. Saminathan, Y. Krishnan, Nat. Nanotechnol. 14 (2018) 176–183.
[28] Y. Hu, Y. Wang, J. Yan, et al., Adv. Sci. 7 (2020) 2000557.
[29] K. Haruta, N. Otaki, M. Nagamine, et al., Nucleic Acid Ther. 27 (2017) 36–44.
[30] D. Thirunavukarasu, T. Chen, Z. Liu, N. Hongdilokkul, F.E. Romesberg, J. Am. Chem. Soc. 139 (2017) 2892–2895.
[31] N.D. Abeydeera, M. Egli, N. Cox, et al., Nucleic Acids Res. 44 (2016) 8052–8064.
[32] C. Riccardi, C. Fabrega, S. Grijalvo, et al., J. Mater. Chem. B 6 (2018) 5368–5384.
[33] Z. Wang, L. Song, Q. Liu, et al., Angew. Chem. Int. Ed. 60 (2020) 2594–2598.
[34] S. Zou, Y. Lei, W. Ma, et al., Analyst 145 (2020) 2562–2569.